

Functionally Optimized Ceramic Structures

C. Gasdaska, R. Clancy, M. Ortiz[#] and V. Jamalabad
AlliedSignal, Inc. Research and Technology
Morristown, NJ 07962

Anil Virkar
Department of Materials Science and Engineering, University of Utah, UT

Dragan Popovitch
Advanced Ceramics Research
Tucson, AZ

The feasibility of using the Fused Deposition of Ceramics (FDC) process to rapidly fabricate functional quality advanced ceramic components has been demonstrated. Multiple extrusion heads enable the deposition of spatially engineered ceramic microstructures on the scale of 250 μm . This unique capability of FDC allows components to be built with combinations of materials and properties that are difficult or impossible to produce using conventional fabrication processes. Some concepts will be presented, along with examples of multiple material laminates produced using FDC. Strength data will be presented which demonstrates the performance improvement possible using spatially engineered microstructures.

Introduction

By suitably combining materials, it is possible to achieve improvements in properties such that the strength and toughness of the combination is greater than that for either material alone. Two multi-material approaches used for strengthening and flaw tolerance in brittle materials are development of residual surface compressive stresses due to coefficient of thermal expansion (CTE) mismatch¹, and fabrication of silicon nitride/ boron nitride fibrous monolith composite structures².

The concept of using combinations of ceramic materials with different coefficients of thermal expansion (CTE) to produce residual stresses on cooling from the fabrication temperature is well documented in the literature¹. Systems which rely on phase changes to produce residual stresses have also been studied³. Strength increases of 300% have been observed in some of these systems. Reliability and flaw tolerance is also improved. In the present work, we are interested in pursuing multi-material combinations which are compatible and co-sinterable with silicon nitride, the leading candidate for high temperature structural applications such as gas turbine engine components. The 1-dimensional aspect of part building using FDC allows for structures more complicated than the simple laminates prepared using traditional methods⁴.

Fibrous monolith (FM) materials are essentially unidirectional composites in which the volume fraction of the matrix material is < 20%. The most common example consists of a

[#] Located at AlliedSignal Engines Division, Phoenix, AZ

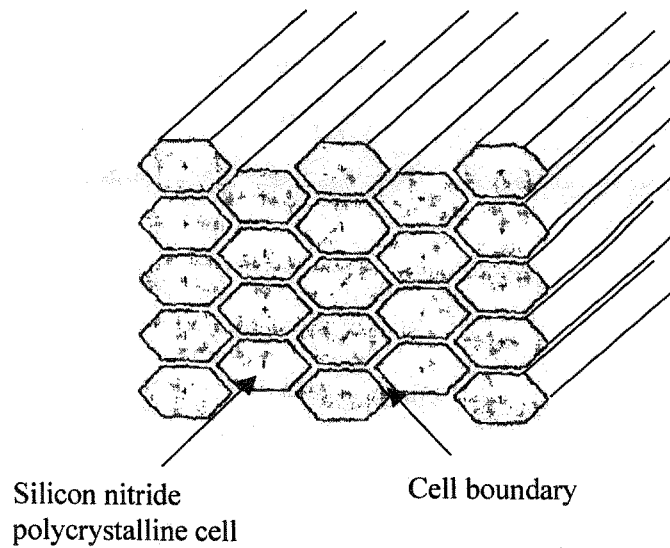


Figure 1. Cross-section of an idealized fibrous monolith microstructure.

structure containing silicon nitride filaments surrounded by a sheath of boron nitride (see Figure 1).

Cracking in these materials tends to be confined to the boron nitride layer, resulting in extensive delamination under bending stresses². Alternatives to boron nitride are being investigated which would allow a greater amount of fiber pullout and work of fracture under tensile loading conditions. Typically, FM materials are produced using filament-winding techniques using fibers which have the FM structure. The FDC process offers a more cost effective method for producing these materials.

The solid freeform fabrication process we are using is based on the Stratasys machine. This technique uses solids loaded filament to deposit roads of a binder/ceramic powder mixture⁴. For multi-material parts, we are using a Stratasys 1650 dual-liquefier rapid prototyping machine.

Laminates

In order to take advantage of the capability of FDC to spatially distribute materials, systems must be found which not only result in desirable material property combinations, such as residual stress production, but which are also capable of being co-sintered without excessive cracking or delamination. Toward this end, we have been examining the use of particulates dispersed in a silicon nitride matrix to increase the CTE. Two candidate material systems for use in silicon nitride are listed in Table 1.

Material	Melting/Decomposition Temperature (°C)	Coefficient of thermal expansion (°C x 10 ⁶)	Young's Modulus (GPa)	Density (g/cm ³)
SiC	2700	4.3	448	3.22
TiN	2940	9.35	260	5.22

Table 1. Properties of candidate particulate dispersants.

In order to evaluate the effectiveness of these materials in strengthening silicon nitride, bi-material laminates were prepared using slip-casting. The materials consisted of silicon nitride and silicon nitride plus up to 30 weight% of either TiN or SiC. The samples were sintered and dense samples were successfully prepared. Test bars were machined and room temperature bending strength measured. Results for samples containing SiC appear in Figure 2. The geometry of the samples is also illustrated. The results indicate that average strength can be increased by up to ~27%. In addition, the decrease in the amount of strengthening at 800 °C is consistent with the drop in residual stress as the test temperature approaches the temperature at which stresses start to set on cooling.

Verification that the increase in strength was due to residual stress was accomplished by a method of progressive material removal and strain measurement using strain gauges. In this technique³ a strain gauge is mounted on a laminated sample and the build-up of strain is monitored as material is progressively removed from the opposite surface. A residual stress of ~157 MPa was measured using this technique. The differential strain between laminate materials

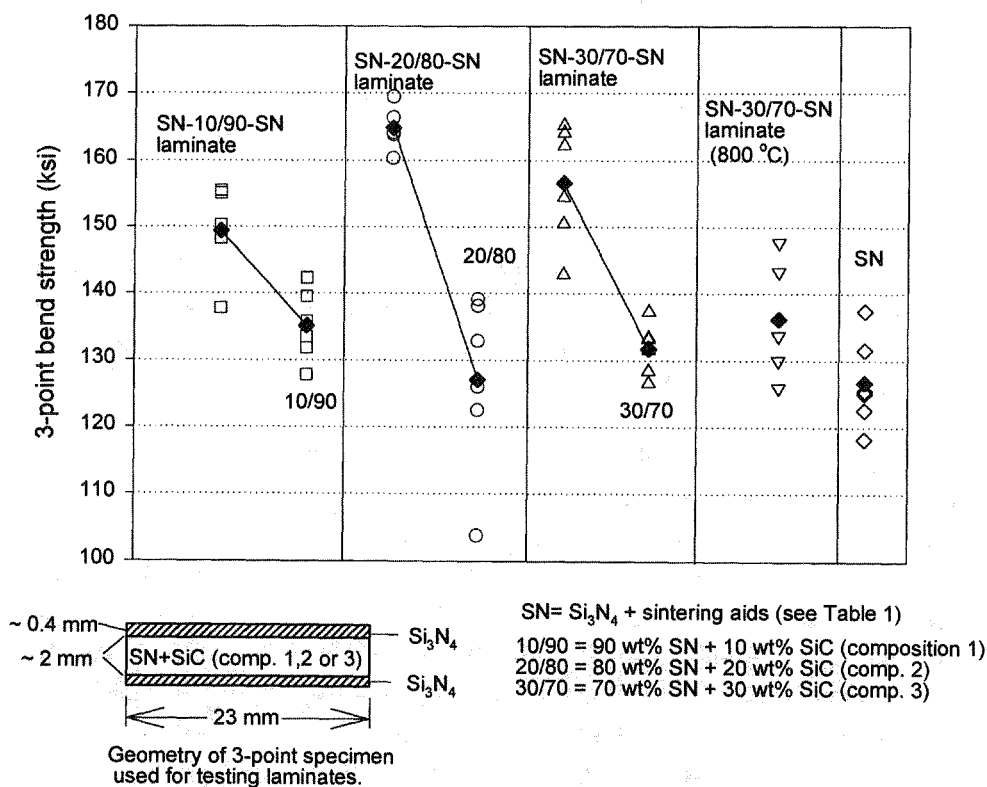


Figure 2. Strength data obtained in 3-point bending for laminates prepared from the indicated compositions. Data for both the laminates and the "core" materials are presented and connected by the lines. Individual data points are plotted, with the average strength for each group represented by the filled diamond symbol. In all cases, the average strength of the core (10/90, 20/80 or 30/70) is less than the laminate strength, indicating strengthening due to surface compressive stresses. The drop in strength at 800 °C is also consistent with the presence of residual stress due to thermal expansion mismatch between the core and outer skins. The strength of the outer skin by itself is shown by the group labeled SN.

was measured as 5.4×10^{-4} . If we assume that on cooling from the sintering temperature permanent stresses begin to set in at 1300°C , then a difference in CTE of $0.42 \times 10^{-6}/^\circ\text{C}$ would produce a differential strain of $\sim 5.4 \times 10^{-4}$.

Using combinations of materials with CTE mismatch to produce residual stresses raises a number of issues. For example, residual stresses must not be so large as to induce spalling or delamination between materials. In addition, the bonding at the interface and the presence of interface defects are important characteristics in determining the ultimate degree of strengthening. The spalling and delamination question is strongly dependent on the interfacial bonding and Mode II fracture energy at the interface. Techniques for measuring interfacial fracture energy are under development. However, for the problem of failure from the surface versus failure at the interface – where residual tensile stresses develop – has been outlined for the case of bending. As an example, assuming a three layer laminate stressed in bending the corresponding fracture strengths (in flexure) are:

$$\sigma_{F(S)} = \sigma_{SF}^o + \frac{d_2 E \Delta \epsilon_0}{(1 - \nu) d}$$

for failure from the surface, and

$$\sigma_{F(I)} = \frac{d}{d_2} \sigma_{IF}^o - \frac{2d_1 E \Delta \epsilon_0}{(1 - \nu) d_2}$$

for failure from the interface. Where, σ_{SF}^o and σ_{IF}^o are the true fracture strengths for failure from surface and interface flaws, respectively, d_1 is the outer layer thickness, d_2 is the inner layer thickness, $d = 2d_1 + d_2$ and $\Delta \epsilon$ is the free strain difference between materials (related to the difference in CTE and ΔT). E is Young's modulus.

The preceding equations show that to maximize the strength as well as the damage resistance, the following are required: (1) high σ_{IF}^o : This can be achieved by improving processing such that interior flaws are kept to a minimum. (Failure from the interior may not be bad either); (2) the inner layer should be fully encapsulated in the outer layer such that there is no chance of introducing damage in the inner layer during service (complete confinement); (3) enhance $\Delta \epsilon_0$ to as high a value as possible such that a high surface compressive stress exists. This provides damage resistance. However, the surface compressive stress should not be so large as to cause delamination; (4) decrease d_1 to a value small enough (relative to d_2) such that interior tensile stress is kept to a minimum, yet d_1 is large enough to prevent contact-induced damage from penetrating too deep into the inner region. Preliminary calculations show an outer layer of thickness ~ 150 to $250 \mu\text{m}$ to be more than adequate for most applications. For a component of 5 mm thickness, the $d_2/2d_1$ ratio is then between 9 and 15.67. For a component of 20 mm in thickness, with an outer layer thickness of $\sim 500 \mu\text{m}$, the ratio is 19. The corresponding tensile stress in the inner layer is very small. This latter example corresponds to the case of the SiC insert being examined by AlliedSignal Engines (see next section), where the insert is located ~ 380 microns below the silicon nitride surface and the overall thickness is $\sim 20 \text{ mm}$.

Design using FDC

While the preceding work has demonstrated the feasibility of using compatible, co-sinterable material combinations for strengthening, the ultimate goal is to use the unique spatial control capabilities of FDC to design and build components. As part of the project on solid freeform fabrication, the Engines division at AlliedSignal (ASE) has been working on designing a multi-material turbine blade which uses residual stress strengthening.

The design used for modeling consists of a ceramic blade inserted in an AF-2 alloy disk (Figure 3). In this initial work, design analysis was focussed on the attachment area since this region is known to experience the highest stresses and contains the area most likely to fail. Stresses in the attachment area were analyzed for a rotational speed of 33,500 RPM and a uniform temperature of 1450 °F. Based on these conditions a uniform stress of 24.1 ksi was imposed outside the attachment area. The coefficient of friction between blade and disk was assumed to be 0.6. This was based on previous experience with ceramic blade attachment systems. Using these inputs, a baseline condition was analyzed. The peak stress was calculated to be 105 ksi and located just outside the contact area between the blade and disk. It arises from the high frictional load between blade and disk.

Various design strategies were evaluated to reduce this peak stress and are illustrated in Figure 3. Although a silicon carbide material has been modeled as the higher CTE component, particulate based silicon nitride composites would provide nearly equivalent behavior. Three of the four geometries examined utilized combinations of SiC and Si₃N₄ to produce residual compressive stresses in the contact area. The geometry illustrated in Figure 3d – a blade containing a central cavity to reduce weight – actually caused a 77% increase in peak stress. Figure 3c illustrates the most promising approach. A silicon carbide insert in the contact area significantly reduces the peak stress.

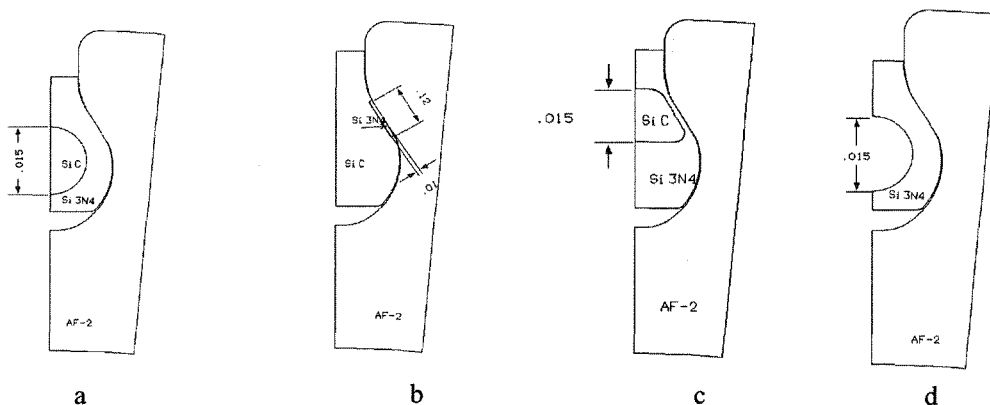


Figure 3. Various geometries evaluated for reducing the peak stress in the contact area.

The amount of the reduction is a function of set temperature; i.e., the temperature at which sufficient rigidity is obtained to start developing residual stress. The higher the set temperature, the larger the residual stress which can be produced by differential contraction. This is shown in

Figure 4, where the maximum stress at 787 C is given as a function of set temperature. Based on a set temperature of 1300 C, the peak stress is reduced from 105 ksi to 72.2 ksi.

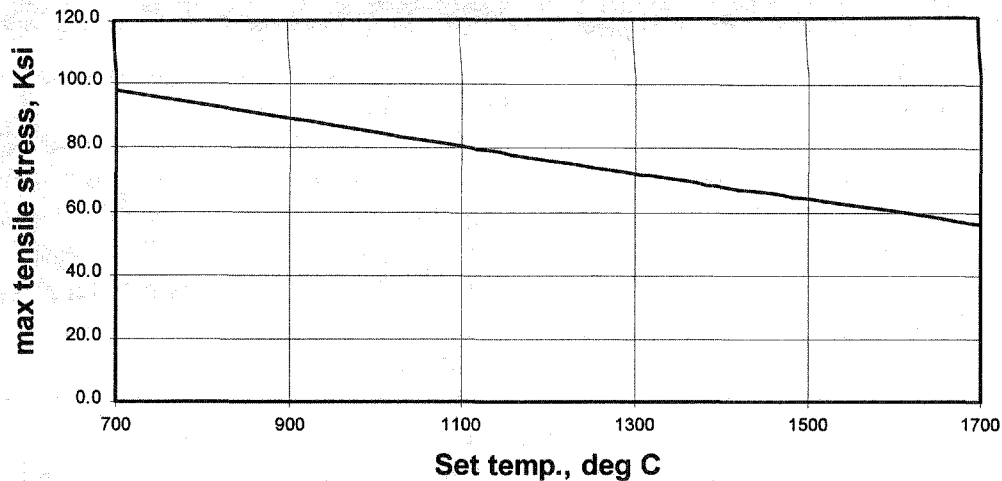


Figure 4. Variation in the maximum tensile stress in the blade attachment area as a function of set temperature.

Fabrication of a complete blade using multi-material FDC is expected to begin shortly. In the meantime, the feasibility of the process has been demonstrated in sub-element testing. Figure 5 shows a cross-section of a turbine blade with a narrow band of insert material at the attachment area.

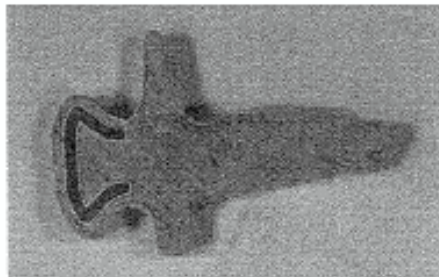


Figure 5. Cross-section of blade built with insert material in the attachment area (black line at right).

Fibrous Monoliths

A major concern regarding the fused deposition of filaments with fibrous monolith structure was whether or not the fibrous monolith structure would be retained as the filament was melted in the liquefier and extruded. In order to address these concerns, Advanced Ceramics Research (ACR) fabricated a fibrous monolith filament containing a single core and sheath, using a model system containing alumina and carbon black for this evaluation. The core material was RU9

(Stratasys, Inc.) binder containing 55 vol% alumina while the sheath consisted of RU9 binder containing 42.75 vol% alumina and 2.25 vol% carbon black. The core and sheath constituted 82.5 and 17.5 vol% of the 0.070 inch diameter filament, respectively.

A number of test pieces were produced and a cross-section of one piece is shown in Figure 6. In order to more clearly discern the structure, the roads in this piece were laid down on

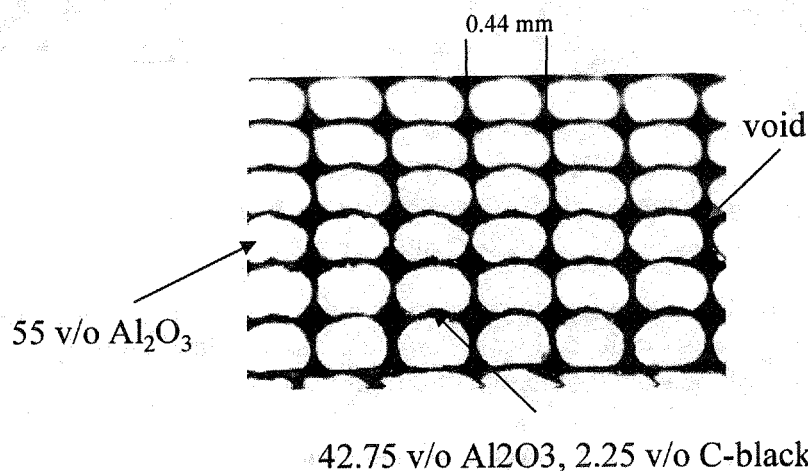


Figure 6. Cross-section of single-cell fibrous monolith sample prepared by fused deposition of fibrous monolith filament.

top of each other, resulting in the voids which appear in Figure 6. As seen in Figure 6, the fibrous monolith microstructure was retained during the deposition process. A 0.015 inch diameter nozzle was used for deposition, resulting in a road width of ~ 0.017 inches. ACR also prepared a 0.070 inch diameter filament containing 12 cells, each with a core and sheath, of alumina and carbon black respectively.

A micrograph of the filament cross-section is shown in Figure 7. The composition of the cell and cell walls was again alumina and alumina/C-black, respectively. The composition of the cell boundary material was adjusted slightly: the solids loading was increased from 45 to 54 volume % solids. Stearic acid was used as the dispersant for both cells and cell walls.

The cell structure retention is excellent after extrusion. Also shown in Figure 7 is a cross-section of a sample built with some overlap between adjacent rows. This overlap is commonly used in FDC to avoid the introduction of strength limiting voids. Though some loss of structure occurs when roads overlap during a build, the overall retention of the FM structure is quite good. Deposition parameters will need to be controlled closely to avoid excessive smearing under these conditions. However, it appears that the microstructural scale obtained (5 micron cell wall thickness) using single cell filament will be sufficient to get the advantages of the fibrous monolith microstructure.

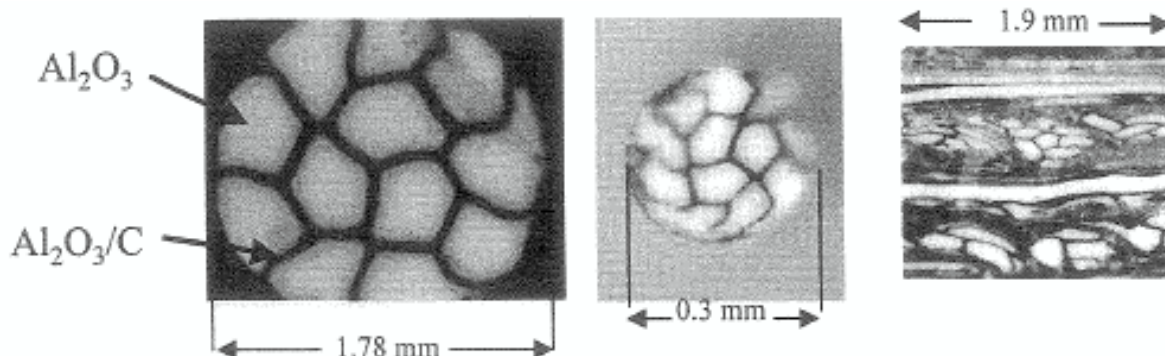


Figure 7. Micrographs of multi-cell fibrous monolith model material showing the structure in the as-prepared filament (left), after extrusion through a 0.3 mm nozzle (center) and after deposition with a 0.076mm overlap between roads (right).

The work on FM structures is being extended to materials based on silicon nitride as the core material and lanthanide glasses for the cell walls. Some promising lanthanide glass compositions have been prepared and will be used to manufacture filament in the next year.

Acknowledgements

The support of DARPA under contract N00014-97-C-0115 is gratefully acknowledged. Also, we would like to thank Sriram Rangarajan of Rutgers University for fabricating the part illustrated in Figure 6, and Don Baskin for his assistance in the preparation of the laminates.

References

1. R. Sathyamoorthy, A. V. Virkar, and R. A. Cutler, *J. Am. Ceram. Soc.*, **75** [5] 1136-1141 (1992).
2. D. Kovar, B. King, R. Trice and J. Halloran, *J. Am. Ceram. Soc.*, **80** [10] 2471-87 (1997)
3. A. Virkar et.al., *J. Am. Ceram. Soc.*, **71** [3] C-148-C-151 (1988)
4. M.K. Agarwala et.al., *Am. Ceram. Soc. Bull.*, **75** [11] 60-65 (1996)